JOURNAL OF MATERIALS SCIENCE 30 (1995) 3091–3097

Microstructural development in the directed melt-oxidized (DIMOX) Al–Mg–Si alloys

V. S. R. MURTHY, B. S. RAO
Department of Materials and Metallurgical Engineering, Indian Institute of Technology, Kanpur 208016, India

Metal–ceramic composites produced via directed melt oxidation (DIMOX) of aluminium alloys are of recent interest. The *in situ* composite forming method is based on the reaction of a molten alloy with a gaseous oxidant. In the present study, Al–Mg–Si alloys were subjected to directed melt oxidation and the progressive microstructural evolution was examined by interrupted growth experiments. In the early stages, liquid alloy oxidizes to form a duplex oxide layer ($MgO + MgAl_2O_4$) on the surface. The openings in these oxide layers allow the liquid alloy to wick through to form small nodules on the surface. When further wicking occurs through these nodules, a "cauliflower" type of colonies is formed. During the early part of the second stage, spinel growth dominates to form a multi-layered structure. In the final stage, as the magnesium reaches low levels, Al_2O_3 formation dominates the growth, and alumina crystals grow continuously for several tens of micrometres. The oxygen required for alumina formation is expected to come from two sources: (i) from the ingress of oxygen through microcracked oxide layers, and (ii) demixing of magnesium-containing oxides in the underneath layers.

1. Introduction

A wide range of metal and ceramic matrix composite materials are being developed to meet the increasing demands from various technological applications, especially from the automotive and aerospace industries. Although a large number of processes have been developed in the past decade [1, 2], several difficulties have been encountered in obtaining controlled microstructures and scaling-up these methods to produce real-life components. Often severe problems are encountered in controlling the interfaces between the matrix and the reinforcement, particularly where reactive matrices and high temperatures are involved. To overcome some of the inherent problems, such as non-wettability, contamination of the reinforcement, undesired interfacial interactions (i.e. from the viewpoint of mechanical properties), novel *in situ* methods have been developed for obtaining metal–ceramic composites [3–10]. The key issue in these *in situ* processes is controlling the material synthesis through optimized reaction kinetics.

In the recent past, the Lanxide corporation, USA, has developed a novel synthesis route, popularly known as the DIMOX (directed melt/metal oxidation) process, to obtain flexible metal–ceramic composites. In DIMOX, Al/Al_2O_3 composite microstructures are obtained via thermal oxidation of a magnesium-containing molten alloy. The liquid alloy oxidizes rapidly at higher temperatures (usually from 1000–1400 °C) and the reaction product grows outwards from the original metal pool surface, either into free space or into a filler material. The growth survives by transportation (wicking) of the liquid alloy through tortuous microscopic channels of the reaction product to reach the oxide–gas interface. The growth proceeds until the metal supply is exhausted or until the reaction front is stopped by an inhibitor barrier coating. The final resultant reaction product is an interconnected α-Al_2O_3 network. Further, the growth kinetics is accelerated by placing filler materials (e.g. particles, whiskers, platelets or fibres) in the path of the reaction front. In this way, a large family of "multiphase" composite materials with varying mechanical properties can be generated [6, 7, 10–12]. The potential advantages of the DIMOX process are simplicity of the process, low processing cost, flexibility in matrix and filler material selection, and the ability to produce complex near-net shapes with desired mechanical properties. Currently, the process is being used successfully to produce a number of engineering components.

To keep the oxidation process alive, the addition of active solute elements such as magnesium, sodium, lithium and zinc (singly or in combination up to quantities of 10 wt%) is desirable. The usefulness of such highly active solute elements is multifold. Besides promoting the wettability, these additions also act as oxygen carriers by undergoing oxidation and dissociation reactions in a cyclic manner, under specified conditions [13]. Although the role is not clearly defined, other minor constituents such as silicon and germanium (mainly group IVA elements) are also believed to improve the wettability and control the kinetics [6].

0022–2461 © *1995 Chapman & Hall*

TABLE I Chemical composition (wt%) of the alloys used for oxidation studies

Alloy	Mg	Si	Impurities Fe, Na, Ca, etc.	Al
A	3.36	2.56	< 0.01	Bal.
B	3.28	9.31	< 0.01	Bal.

In addition to chemistry of the melt, the growth rate is also influenced by oxidizing temperature and time and, to a certain extent, by the partial pressure of oxygen. Oxidation temperatures below 950 °C result in only selective conversion of magnesium to MgO or $MgAl_2O_4$, whereas temperatures above 1400 °C lead to the formation of porous materials. While examining a complex alloy, Nagelberg [14] noted that oxygen partial pressure difference has very little influence on the growth rate, whereas in another investigation on Al–10 wt% Si–2 wt% Mg alloy, growth was found to be dependent on the partial pressure of oxygen ($\alpha \sim P_O^{1/3}$) at temperatures less than 1250 °C [15]. Thus the effect of partial pressure of oxygen appears to be alloy dependent. Activation energies of about 400 kJ mol^{-1} were found for directed melt oxidation with reaction rates of about 2×10^{-5} g cm^{-2} s^{-1} at about 1100 °C [9].

Many investigators have studied different aspects of directed melt oxidation in binary, ternary and even multicomponent, complex alloys [7, 14, 15]. However, only limited investigations have been published on microstructural aspects relating to growth behaviour and formation of Al/Al_2O_3 in Al–Mg and Al–Mg–Si alloys. The present investigation was aimed at studying microstructural development during the oxidation of Al–Mg–Si alloys. Various observations made during the interrupted growth of Al–Mg–Si alloys are presented here.

2. Experimental procedure

Two different aluminium alloys with varying silicon content were prepared using 99.9% pure aluminium, magnesium and silicon. The alloys were prepared by conventional melting methods in a clay–graphite crucible and were cast into 25 mm rods. The chemical analysis of the cast alloys is shown in Table I. The cast rods were cut into appropriate lengths for the oxidation experiments. Oxidation studies were carried out in a precoated (barrier coating was given to prevent the infiltration through the crucible walls) alumina crucible at 1140 ± 5 °C in air for different time intervals (i.e. from 2–24 h). After oxidation, sections were cut parallel to the growth direction and polished samples were examined optically and by scanning electron microscopy (Jeol 840A) using energy dispersive X-ray analysis (EDAX). For X-ray studies (Seifert, Debyeflex 2002; CuK_α) either a thin portion of the oxidized surface or ground powders were used. For identifying the sequence of layers and their chemical composition, backscattered electron imaging was supplemented by EDAX and X-ray analyses.

3. Results

3.1. Macroscopic observations

In the early stage of oxidation, a dark, uneven oxide layer formed on the surface and the original shiny metallic luster of the alloy changed to a dull grey colour. X-ray and EDAX analyses on the surface confirmed the oxide to be MgO. When interrupted oxidation was continued on the same sample (alloy B, Table I), after 5 h the liquid alloy had wicked through openings in the MgO layer. The liquid which had wicked through in early stages had again completely undergone oxidation forming an MgO layer on the surface (globule A, Fig. 1a) whereas in the other nodule (marked B), wicking as well as oxidation are still in progress. A variation in the dimensions of the nodules was seen from time to time. As the oxidation continued for a long time (12 h), a large number of other nodules was generated around the original nodule and the surface was physically modified into a large "cauliflower" type of colony (Fig. 1b). A magnified view of one such nodule is shown in Fig. 1c. However, variations have been observed in the morphology depending on the alloy, temperature and time. In the beginning, growth was predominantly at the boundaries. As the time progressed (after 24 h), the coalescence of such large colonies gave rise to a planar growth front, especially in the central portions of the sample (Fig. 1d). A similar growth sequence was also observed in alloy A.

3.2. Microstructural observations

For better insight of the process, the oxidized globule (marked A in Fig. 1a) was cut parallel to the growth direction and various layers, starting from the alloy reservoir to the top MgO layer, were analysed by EDAX. The surface was found to be covered with MgO as observed earlier. Below this layer, due to reaction of aluminium or Al_2O_3 with MgO, $MgAl_2O_4$ (spinel) has formed (Fig. 2). The spinel layer adjacent to the liquid alloy can be easily identified with metal-filled channels with an irregular reaction front. The liquid metal at any point in time appears to be in touch with the alloy reservoir through fine microchannels (Figs 2 and 3), and in cross-section the metal is seen as isolated and uniformly spaced precipitates (Fig. 2b). The spinel layer away from the liquid alloy/spinel interface is dense and appears as a dark band in the backscattered electron micrograph (Figs 3a and 4). The number of spinel layers (porous and dense) and their thickness varied depending on the location and size of the nodule. Further, the liquid alloy from the reservoir wicked through micro-openings of the duplex (MgO + spinel) layer and formed a number of satellite droplets at the periphery of the nodule (Fig. 2). As time progressed, the size and number of droplets multiplied to give a "cauliflower" type of colony. The alloy reaching the front droplet further undergoes oxidation and the process described above (MgO and $MgAl_2O_4$ formation) is again repeated. In a magnified view, the flow pattern of liquid alloy, spinel and residual alloy are distinctly visible (Fig. 2). No Al_2O_3 formation was detected at this stage.

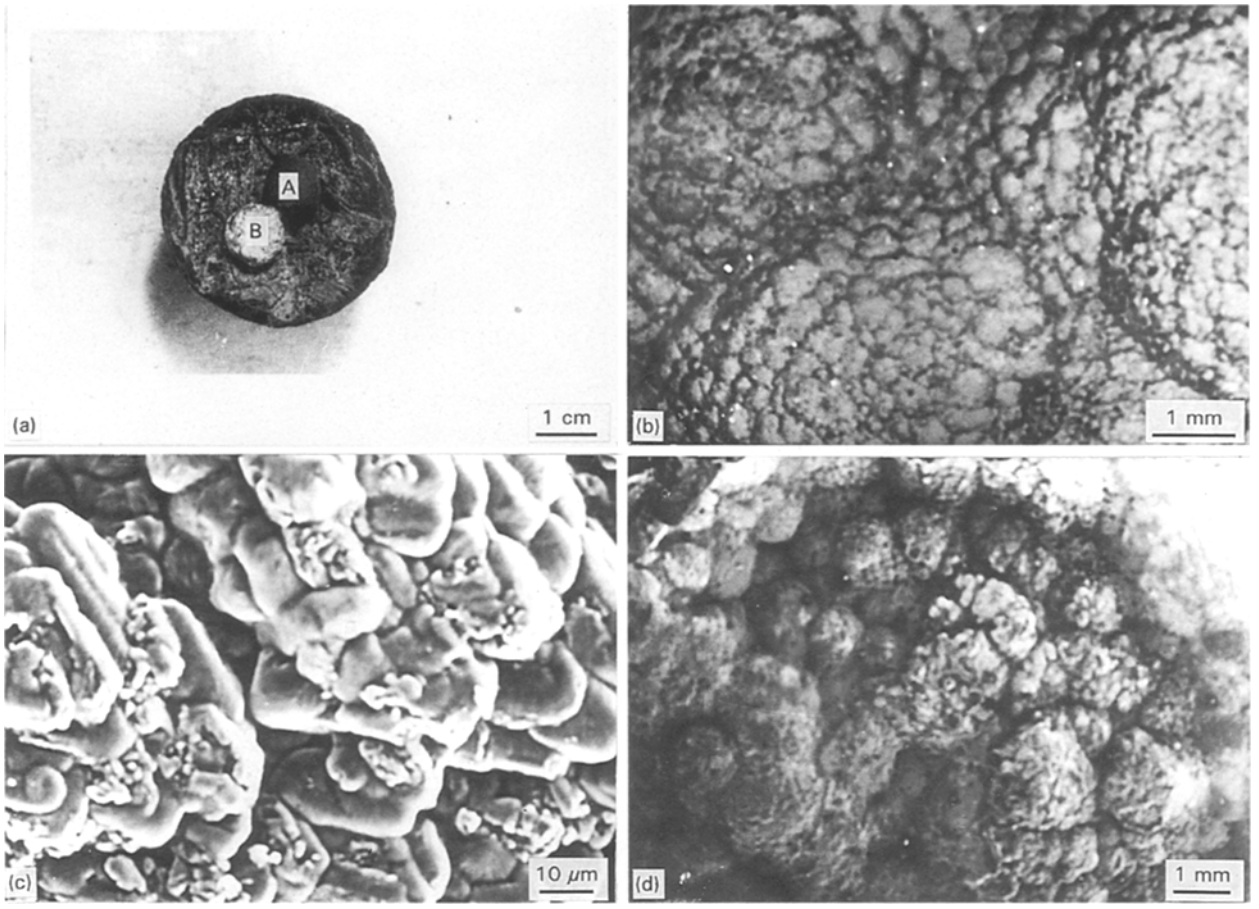

Figure 1 Macroscopic changes in an Al–Si–Mg alloy (alloy B) oxidized at 1140 °C: (a) after 5 h (note the formation of nodules through wicking of liquid alloy); (b) nodules have grown into a "cauliflower" type of colony after 12 h; (c) a magnified view of one of the colonies; (d) planar growth in the central portion of a sample oxidized for 24 h.

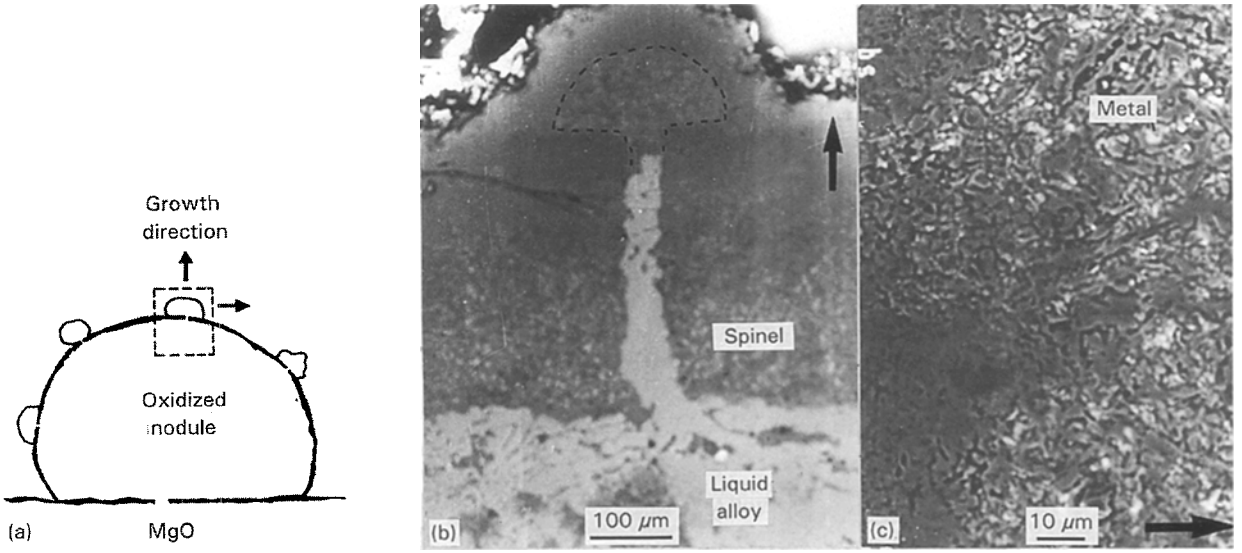

Figure 2 (a) Magnified view of nodule A (in Fig. 1a) when sectioned along the growth direction. Several droplets were seen along the periphery of the nodule. (b) Back-scattered electron (bs) micrograph of a selected area in (a). (c) The liquid alloy in the droplet becomes oxidized to $MgAl_2O_4$. Residual metal and microcavities, due to shrinkage, are distinctly visible.

With continuation of a similar oxidation process for several hours (12 h) in alloy A, growth of a metal–Al_2O_3 composite structure was observed (Fig. 4). At this stage, the composite has grown to a few hundreds of micrometres (a similar growth sequence was also seen in alloy B) and the growth front is still active with continuation of oxidation (Fig. 3c and d). A detailed examination of the oxidation process in the droplets revealed the formation of a duplex layer on the surface of each nodule. However, the thickness (10–15 μm) of the duplex layer is much less than that of the spinel layer formed in the early stages of oxidation. In some of the nodules, the surface duplex layer underwent microcracking (Fig. 3d),

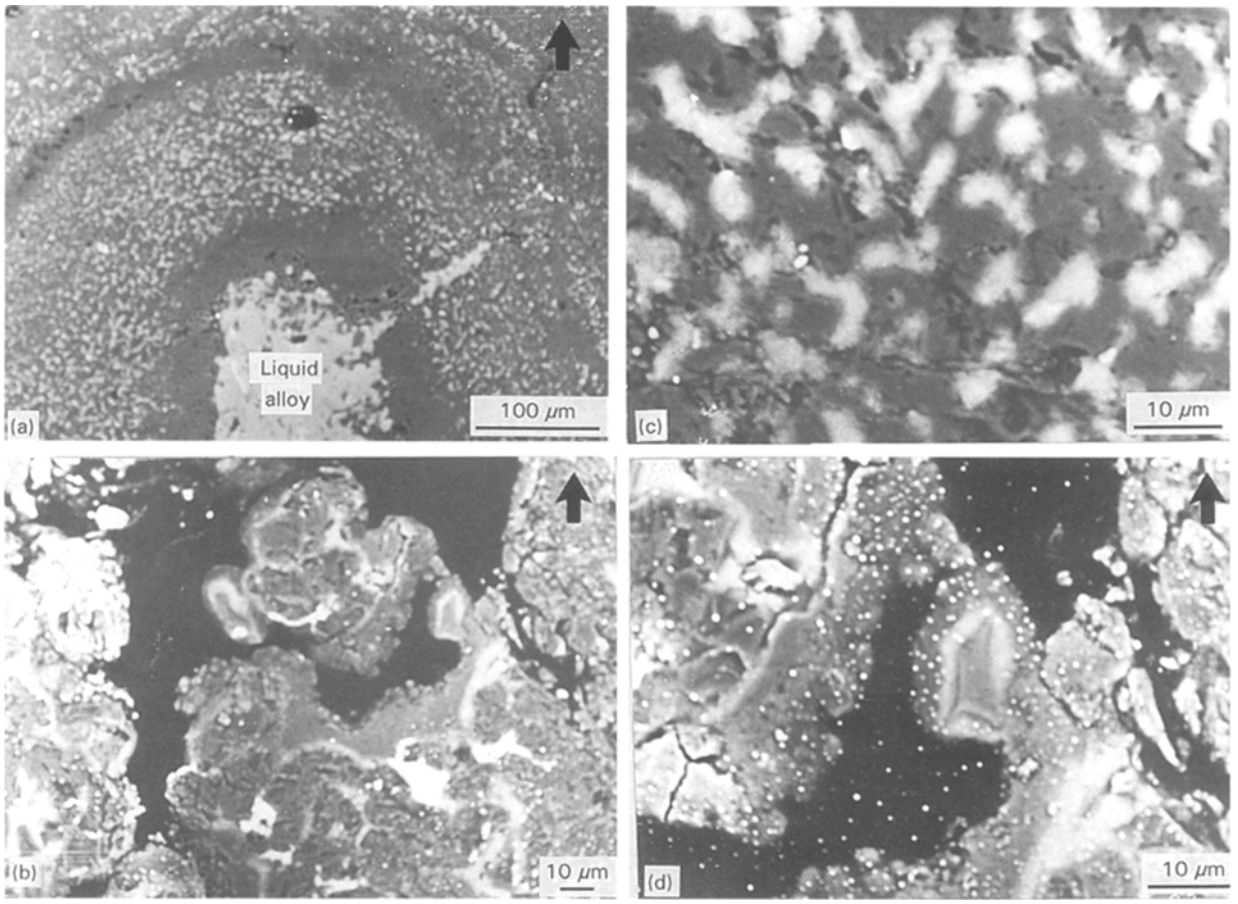

Figure 3 (a) Multiple-layered spinel microstructure in alloy A after oxidizing for 8 h at 1140 °C. (b) Metal-filled spinel layer with interconnected microcracks. (c, d) Active oxidation in the wicked alloy nodules. Arrows indicate the growth direction.

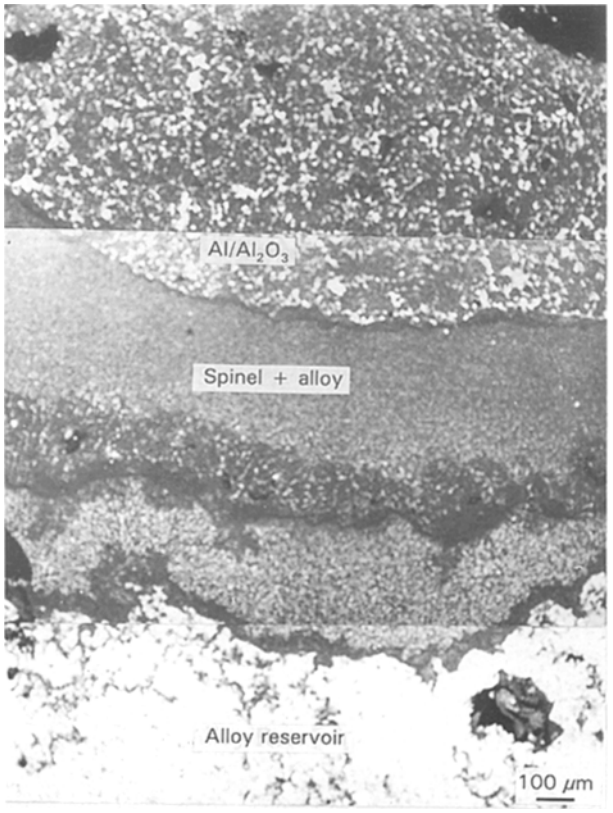

Figure 4 Backscattered electron micrograph of a polished section parallel to the growth direction of alloy A oxidized for 12 h at 1140 °C showing the sequence of various layers formed during the growth process.

permitting easy ingress of oxygen into the nodule, and thus encouraging the growth of Al_2O_3. With time (after 18 h), the growth of Al/Al_2O_3 dominated the structure and in subsequent stages, the surface MgO layer thickness was reduced to $\sim 2\,\mu m$. The silicon (seen as bright spots in Fig. 3c and d) precipitated uniformly throughout the composite structure but did not participate in the oxidation process. This is consistent with the earlier observations made by Nagelberg [15].

More detailed observations were made on Al_2O_3 growth in alloy B. Al_2O_3, which has initially nucleated, continues to grow several tens of micrometres and as the growth progressed, branching of Al_2O_3 was observed from the main column (Fig. 5a). In some instances, where there are microcavities, Al_2O_3 growth could be seen far ahead of the remaining liquid (Fig. 5b). Depending on the location, there are small variations in thickness of these Al_2O_3 crystals. The alloy underneath easily penetrates the fine capillaries that are formed in between the columns of Al_2O_3 (Fig. 5c). The liquid which is being transported through the capillaries contains small proportions of magnesium and silicon, as seen from the analysis.

4. Discussion

The oxidation of Al–Mg alloys is quite complex and has been a subject of study for several years [16–18]. When Al–Mg or Al–Si–Mg alloy is subjected

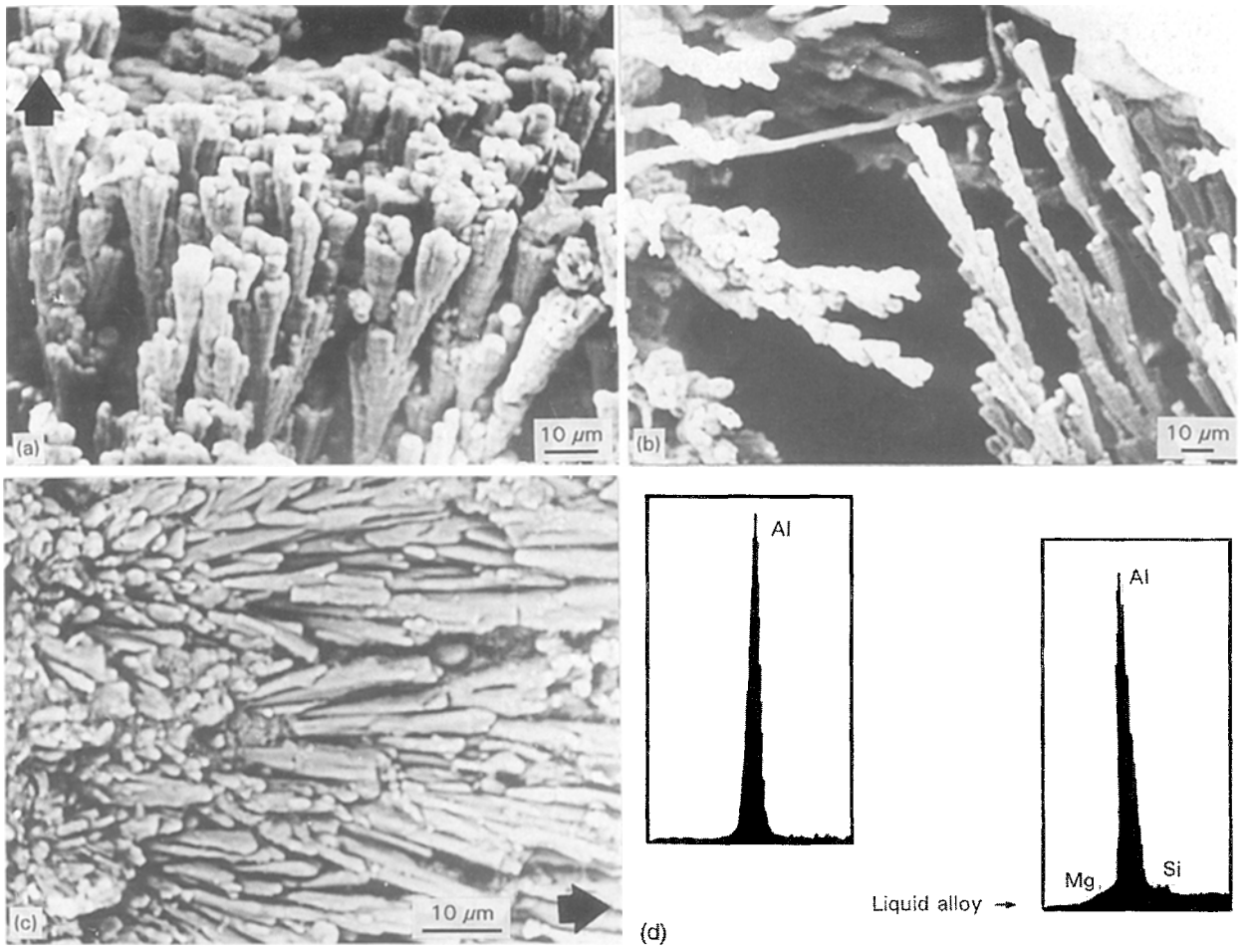

Figure 5 (a) A three-dimensional view of Al_2O_3 crystals and their extensive interconnected branchings during growth. (b) Al_2O_3 growth far ahead of the liquid front. (c) An enlarged view of the Al/Al_2O_3 composite. The residual alloy in between the Al_2O_3 crystals exhibits a composition with low levels of magnesium and silicon.

to thermal oxidation, magnesium depletes from the bulk alloy forming a non-uniform, dark-grey MgO layer on the surface. In aluminium alloys, a magnesium concentration above 1 at % is believed to encourage MgO formation by suppressing continuous, adherent and non-porous layer of Al_2O_3 [19]. MgO with a Pilling–Bedworth ratio of 0.81 does not form a continuous layer on the surface, and hence both out-diffusion of magnesium to the top and in-diffusion of oxygen to the inner reaction front persist as the process continues. In fact, the formation of such a non-protective oxide layer is an essential prerequisite for continuous oxidation of molten alloy and provides a life-line for the formation of metal–ceramic composites at a later stage of oxidation.

Further, aluminium or its oxide in the underneath (magnesium-depleted) alloy reacts with MgO and $MgAl_2O_4$ is formed according to one or both of the following interactions [20]

$$3MgO + 2Al \rightarrow Al_2O_3 + 3Mg \quad (1)$$

$$MgO + Al_2O_3 \rightarrow MgAl_2O_4 \quad (2)$$

$$\text{or } 4MgO + 2Al \rightarrow MgAl_2O_4 + 3Mg \quad (3)$$

The remaining magnesium will re-evaporate to form MgO on the surface. Thus formation and growth of MgO and $MgAl_2O_4$ (with consumption of MgO) are interdependent and competing reactions. However, appearance of MgO on the surface, at any time suggests that MgO formation is more rapid and predominant. During continuous oxidation of alloys, $MgAl_2O_4$ formation can be easily identified by a sharp increase in the weight gain rate in thermogravimetric analysis [21]. The spinel formed due to the above reactions contains interconnected porosity and the pores are filled with liquid alloy. The alloy maintains its continuous contact with the main liquid reservoir underneath (Figs 2 and 3) through interconnected channels. Salas *et al.* [20] speculated that the formation of channels in the spinel is due to (a) some form of morphological instability at the spinel/metal interface, or (b) entrapment of liquid metal in a fast-moving oxidation front in the early stages of oxidation. Additionally, volume change associated with the conversion of MgO to $MgAl_2O_4$ leaves the remaining MgO in compression, which results in buckling and microcracking of MgO. During conversion to $MgAl_2O_4$, the stresses generated (and hence cracking) are expected to be maximum at the periphery of the crucible walls and hence the wicking of liquid (and growth rate) is higher at these points. As the liquid wicks through the initial duplex layer, $MgAl_2O_4$ growth continues to form a large number of dense and porous layers, reacting with the top MgO layer. The number of layers depends mainly on the availability of the

liquid alloy and the magnesium concentration level in the liquid.

As long as the concentration of magnesium in the liquid alloy remains very high, spinel dominates the growth. When the "Mg" concentration reaches $MgAl_2O_4 + Al_2O_3 + (Al, Mg)$ phase field in the Al–Mg–O ternary diagram [20, 22], externally the nodules are covered with $MgO + MgAl_2O_4$ layers and inside the growth of Al/Al_2O_3 composite begins (Fig. 3c and d). Further, when the concentration drops below 0.3 wt%, Al/Al_2O_3 composite microstructure completely dominates the structure and a very thin layer of MgO forms on the surface. However, from the observations in this study, it is not clear exactly where the nucleation of Al_2O_3 occurs. Once the nucleation of Al_2O_3 takes place, growth continues for several tens of micrometres with branching, as shown in Fig. 5. The growth of Al_2O_3 (in α-form) was found to be epitaxial with a large number of low-angle boundaries of $< 5°$, as revealed by Laue back-reflection X-ray and transmission electron microscopy [8]. The liquid with a small amount of magnesium and silicon, easily wets Al_2O_3 and reaches the growth front by capillary action. Although two different silicon-containing alloys were used in this study, the role of silicon during oxidation is not clear from these observations. However, the presence of silicon is expected to (a) improve wettability of the liquid by decreasing the wetting angle, especially when present together with magnesium, decrease the surface tension marginally by controlling the activity of magnesium [22], (b) increase the oxidation of molten aluminium [23, 24], (c) increase the driving force for dissociation of MgO and $MgAl_2O_4$ [20, 21] and finally (d) it may also influence the transport of oxygen through the liquid.

The interesting feature of the growth is the dissociation of oxide layers in the magnesium-depleted alloy. On the surface, at the reaction front, MgO is quite stable, but as we move down away from the reaction growth front, both surface oxide layers, i.e. MgO and $MgAl_2O_4$, dissociate and the structure appears to be a continuous Al/Al_2O_3 microstructure. Schmalzried and Laqua [25] showed (thermodynamically and experimentally) that under an oxygen potential gradient, multicomponent oxides tend to demix depending on the relative mobilities of the constituents and the faster diffusing species is enriched at the higher oxygen activity side of the oxide. In this context, Mg^{2+}, which diffuses at a higher rate, would tend to reach the reaction front to form an MgO surface layer. The dissolved oxygen is expected to facilitate Al_2O_3 growth [13, 20]. Further, the oxygen gradient in the metal layer ahead of the advancing Al_2O_3 interface is supposed to create conditions which may favour perturbations on the growing Al_2O_3 surface (Fig. 5).

5. Conclusion

Various stages in the microstructural development of directed melt-oxidized Al–Si–Mg alloys was studied by interrupted growth experiments. In the initial stages of oxidation, the molten alloy rapidly oxidizes to form an MgO layer. MgO further reacts with aluminium to form $MgAl_2O_4$. The oxidation front maintains contact with the underlying main liquid reservoir through narrow liquid channels. Further, the microcracks or porosity in the oxide layers give way to the liquid alloy and small nodules are formed on the surface. The nodules grow into large colonies as the liquid finds its way through tortuous paths. At this stage, multiple layers of spinel (both porous and dense) form, giving rise to a multiple banded structure. As the process continues and the magnesium concentration reaches the $MgAl_2O_4 + Al_2O_3 +$ liquid alloy (Mg, Al) equilibrium phase field, the beginning of the Al/Al_2O_3 composite structure is seen. When the magnesium concentration drops further, Al_2O_3 growth completely dominates the structure, and the oxygen required for oxidation is supplied either by ingress of oxygen through microcracks formed on the nodules, or by the demixing of magnesium-containing oxides under an oxygen potential gradient.

Acknowledgements

The financial assistance received from BRNS, India, is gratefully acknowledged. The authors are also grateful to Professor G. S. Murty for his valuable suggestions.

References

1. S. RAY, *J. Mater. Sci.* **28** (1993) 5397.
2. R. K. EVERETT and R. J. ARSENAULT, "Metal matrix composites: Processing and interfaces" (Academic Press, San Diego, USA, 1991).
3. M. J. KOCZAK and M. K. PREMKUMAR, *J. Metals* **45** (1993) 44.
4. E. USTUNDAG, R. SUBRAMANIAN, R. VAIA, R. DIECKMANN and S. L. SASS, *Acta Metall. Mater.* **41** (1993) 2153.
5. R. K. VISWANADHAM, J.D WHITTENBERGER, S. K. MANNAN and B. SPRISSLER, *Mater. Res. Soc. Symp. Proc.* **120** (1988) 89.
6. M. S. NEWKIRK, H. D. LESHER, D. R. WHITE, C. R. KENNEDY, A. W. URQUHART and T. D. CLARR, *Ceram. Eng. Sci. Proc.* **8** (1987) 879.
7. M. K. AGHAJANIAN, N. H. MACMILLAN, C. R. KENNEDY, S. J. LUSZCZ and R. ROY, *J. Mater. Sci.* **24** (1989) 658.
8. M. S. NEWKIRK, A. W. URQUHART, H. R. ZWICKER and E. BREVAL, *J. Mater. Res.* **1** (1986) 86.
9. H. SCHOLZ and P. GREIL, *J. Mater. Sci.* **26** (1991) 669.
10. M. K. AGHAJANIAN, J. T. BURKE, D. R. WHITE and A. S. NAGELBERG, *SAMPE Q.* **20** (1989) 43.
11. P. BARRON-ANTOLIN, G. H. SCHIROKY, C. A. ANDERSON, *Ceram. Eng. Sci. Proc.* **9** (1988) 759.
12. C. A. ANDERSSON, P. BARRON-ANTOLIN, G. H. SCHIROKY and A. S. FAREED, "International Conference on Whisker- and Fibre-toughened Ceramics", Oak Ridge, Tennesee, June 1988.
13. S. ANTOLIN, A. S. NAGELBERG and D. K. CREBER, *J. Am. Ceram. Soc.* **75** (1992) 447.
14. A. S. NAGELBERG, *Solid State Ionics* **32/33** (1989) 783.
15. A. S. NAGELBERG, S. ANTOLIN and A. W. URQUHART, *J. Am. Ceram. Soc.* **75** (1992) 455.
16. R. A. HINE and R. D. GUMINSKI, *J. Inst. Metals* **89** (1961) 417.
17. M. H. ZAYAN, O. M. JAMJOOM and N. A RAZIK, *Oxid. Metals* **34** (1990) 323.
18. C. N. COCKRAN, D. L. BELITSKUS and D. L. KINOSZ, *Metall. Trans.* **8B** (1977) 323.

19. G. M. SCAMANS and E. P. BUTLER, *ibid.* **6A** (1975) 2055.
20. O. SALAS, H. NI, V. JAYARAM, K. C. VLACH, C. G. LEVI and R. MEHRABIAN, *J. Mater. Res.* **6** (1991) 1964.
21. K. C. VLACH, O. SALAS, H. NI, V. JAYARAM, C. G. LEVI and R. MEHRABIAN, *ibid.* **6** (1991) 1982.
22. D. A. WEIRAUCH Jr, *ibid.* **3** (1988) 729.
23. W. THIELE, *Aluminium* **38** (1962) 707.
24. *Idem, ibid.* **38** (1962) 780.
25. H. SCHMALZRIED and W. LAQUA, *Oxid. Metals.* **15** (1981) 339.

Received 30 June 1994
and accepted 9 January 1995